Published OnlineFirst April 2, 2014; DOI: 10.1158/2326-6066.CIR-13-0202

Research Article

Cancer Immunology Research

ERK-Dependent Downregulation of the Atypical Chemokine Receptor D6 Drives Tumor Aggressiveness in Kaposi Sarcoma

Benedetta Savino[1,2], Nicoletta Caronni[1,2], Achille Anselmo[1], Fabio Pasqualini[1], Elena Monica Borroni[1,2], Gianluca Basso[1], Giuseppe Celesti[1], Luigi Laghi[1], Athanasia Tourlaki[4], Vinicio Boneschi[4], Lucia Brambilla[4], Manuela Nebuloni[3], Gianluca Vago[3], Alberto Mantovani[1,2], Massimo Locati[1,2], and Raffaella Bonecchi[1,2]

Abstract

D6 is an atypical chemokine receptor acting as a decoy and scavenger for inflammatory CC chemokines expressed in lymphatic endothelial cells. Here, we report that D6 is expressed in Kaposi sarcoma (KS), a tumor ontogenetically related to the lymphatic endothelium. Both in human tumors and in an experimental model, D6 expression levels were inversely correlated with tumor aggressiveness and increased infiltration of proangiogenic macrophages. Inhibition of monocyte recruitment reduced the growth of tumors, while adoptive transfer of wild-type, but not CCR2$^{-/-}$ macrophages, increased the growth rate of D6-competent neoplasms. In the KS model with the B-Raf V600E–activating mutation, inhibition of B-Raf or the downstream ERK pathway induced D6 expression; in progressing human KS tumors, the activation of ERK correlates with reduced levels of D6 expression. These results indicate that activation of the K-Ras–B-Raf–ERK pathway during KS progression downregulates D6 expression, which unleashes chemokine-mediated macrophage recruitment and their acquisition of an M2-like phenotype supporting angiogenesis and tumor growth. Combined targeting of CCR2 and the ERK pathway should be considered as a therapeutic option for patients with KS. *Cancer Immunol Res; 2(7); 679–89. ©2014 AACR.*

Introduction

Chemokines are a superfamily of inflammatory mediators supporting cell migration and leukocyte activation through a distinct family of class A G protein–coupled receptors (GPCR; refs. 1, 2). Besides these canonical receptors, which support chemotactic activity, there is a separate group of atypical chemokine receptors that do not directly mediate cell migration but are still involved in leukocyte recruitment as they participate in chemokine gradient formation by trapping, degrading, or transporting their ligands (3, 4). D6 is an atypical chemokine receptor operating as a decoy and scavenger receptor for most inflammatory CC chemokines, and its role in the control of inflammatory responses is well established (3, 5). D6-deficient mice have been reported to have increased susceptibility to skin carcinogenesis (6) and colitis-associated cancer (7), thus providing genetic evidence of a nonredundant function of inflammatory chemokines in tumor biology (8–11). D6 is selectively expressed in lymphatic endothelial cells (LEC) and in a subset of vascular tumors (12), but its role in these malignancies is unknown.

Kaposi sarcoma (KS) is a vascular tumor caused by the infection of LECs by the human herpes virus 8 (HHV8). KS tumor cells, also referred to as spindle cells for their shape, are considered to be derived from the LEC lineage and express several LEC markers, including VEGFR3, LYVE-1, and PROX1 (13). It has been shown that KS can also derive from HHV8-infected blood vascular cells that undergo a lymphatic reprogramming to create a more favorable microenvironment for tumor growth (14). Even though HHV8 infection is widespread, KS occurs only sporadically in immunocompetent individuals as classical KS, which is usually characterized by slow-progressing skin lesions with limited dissemination ability. However, KS is relatively common in immunocompromized patients; it displays a more aggressive phenotype with widespread diffusion on the skin, frequent involvement of visceral organs, and life-threatening complications (15). As current therapeutic options are only palliative, KS is a leading cause of morbidity and mortality in patients with AIDS (16, 17).

KS lesions appear as multiple foci highly heterogeneous in their composition depending on the disease stage. The first lesions detectable in the dermis, called patch lesions, are

Authors' Affiliations: [1]Humanitas Clinical and Research Center; [2]Department of Medical Biotechnologies and Translational Medicine, Università degli Studi di Milano, Rozzano; [3]Department of Clinical Sciences "Luigi Sacco," Università degli Studi di Milano; and [4]UO Dermatologia, Fondazione IRCCS Ca' Granda, Ospedale Maggiore Policlinico, Milano, Italy

Note: Supplementary data for this article are available at Cancer Immunology Research Online (http://cancerimmunolres.aacrjournals.org/).

B. Savino, N. Caronni, A. Mantovani, M. Locati, and R. Bonecchi contributed equally to this work.

Corresponding Author: Raffaella Bonecchi, Department of Medical Biotechnologies and Translational Medicine, University of Milan School of Medicine, Via Manzoni 56, I-20089 Rozzano, Milano, Italy. Phone: 39-02-82245117; Fax: 39-02-82245101; E-mail: raffaella.bonecchi@humanitasresearch.it

doi: 10.1158/2326-6066.CIR-13-0202

Published OnlineFirst April 2, 2014; DOI: 10.1158/2326-6066.CIR-13-0202

composed of a few HHV8-infected spindle cells, an abundant inflammatory infiltrate mainly containing T and B lymphocytes and monocytes, and a prominent angiogenic process. Then lesions progress to the plaque stage, characterized by lesions that are solid, edematous, and violaceous in color, and finally to maculonodular lesions, with abundant abnormal leaky vessels with edema and erythrocyte extravasation and a predominance of spindle cells (18). KS lesions are classified in four clinical stages (I, maculonodular lesions; II, infiltrative; III, florid; and IV, disseminated). Lesions at the same stage show a highly variable progression rate and are further subdivided retrospectively according to the speed of disease evolution (A, slow progressive lesions, and B, rapid progressive lesions; ref. 19).

Spindle cells do not display some characteristics of transformed cells, being euploid and not clonal, and with a growth potential *in vitro* and *in vivo* largely dependent on the autocrine/paracrine activity of angiogenic and inflammatory cytokines, including VEGF-A, basic fibroblast growth factor 2 (bFGF2), interleukin (IL)-6, and IL-1β (15, 20). It has been proposed that spindle cells produce cytokines that recruit leukocytes and vessels, which in turn produce growth factors required for their proliferation (18, 21, 22). Consistent with this, KS lesions often occur at inflammatory sites or in scarring tissues, a condition known as Koebner phenomenon, and in patients with the immune reconstitution inflammatory syndrome (23). Among inflammatory mediators, chemokines have been investigated extensively in KS pathogenesis because HHV8 has hijacked the chemokine system in several ways (24). HHV8 encodes a constitutively active GPCR, recognizing both angiostatic, i.e., without the Glu–Leu–Arg amino acid motif (ELR^-) and angiogenic ELR^+ CXC chemokines, which act as transforming receptors in transgenic mice (25), and three CC chemokines (vMIP-I, -II, and -III) that interact with the CCR3, CCR8, and CCR4 receptors that are expressed at high levels in Th2 and regulatory T cells (Treg; refs. 26, 27); these viral inflammatory CC chemokines represent a strategy to subvert and divert effective antiviral and antitumor immunity. In addition, HHV8-infected endothelial cells display increased production of several chemokines, including CCL2, CCL5, CXCL8, and CXCL16 (28, 29).

Considering the lymphatic origin of KS and the relevance of the chemokine system in its biology, we investigated the expression and the role of the atypical chemokine receptor D6 in this tumor.

Materials and Methods

Immunohistochemistry

Formalin-fixed paraffin-embedded cutaneous nodular KS lesions from HIV-seropositive and -seronegative cases were obtained from Luigi Sacco Hospital and Ospedale Maggiore Policlinico (Milan, Italy), respectively. Cutaneous nodular KS lesions from HIV-seronegative patients were classified according to a staging system (19) comprising four clinical stages (I, maculonodular lesions; II, infiltrative; III, florid; and IV, disseminated), each further divided according to the speed of disease evolution (A, slow, and B, rapid). Ethics approval for D6 expression analysis was obtained from the local Institutional Review Committee, and a signed informed consent was obtained from all participants. Sections were incubated with rat anti-human D6 monoclonal antibody (mAb; clone 196124, 1:100 dilution; R&D Systems) and mouse anti-human KSHV Orf73 mAb (1:100 dilution; Dako). For murine tumors, frozen sections were incubated with rat anti-mouse CD31 mAb (1:100 dilution; obtained as described in ref. 30).

Cell culture and transfection

The KS-IMM cell line, originally isolated from a KS from a kidney-transplanted immunosuppressed patient (31), was grown in Dulbecco's Modified Eagle Medium (DMEM; Lonza) with 10% fetal calf serum (FCS). KS-IMM cells were transfected with the hD6/pEFGP-N1 or empty pEFGP-N1 expression plasmids by using Lipofectamine 2000 (Invitrogen) and selected using 400 μg/mL G418 (Invitrogen). For growth curve, KS-IMM cells were seeded in 6-well plates (5×10^4 cells/well) and grown under normal conditions for 1 to 4 days. Every day, cells were harvested with trypsin from 3 wells per group, diluted in Trypan blue to assess viability, and counted. For the preparation of cell culture supernatant, KS-IMM cells (1×10^6 cells) were cultured in 75-cm^2 flasks with complete medium. After 48 hours, culture medium was discarded, and fresh medium without G418 was added to the flask for 24 hours. Supernatant was collected and centrifuged.

Immunofluorescence microscopy analysis

KS-IMM cells (10^5) were seeded in 24-well plates and grown at 37°C for 18 hours. Cells were fixed with 4% paraformaldehyde and then incubated with 4′,6-diamidino-2-phenylindole (DAPI). High-resolution images (1,024 × 1,024 pixels) were acquired sequentially with a 60×/1.4 NA Plan-Apochromat oil immersion objective using a FV1000 laser scanning confocal microscope (Olympus). Differential interference contrast (Nomarski technique) was also used. Images were assembled and cropped using Photoshop software (Adobe Systems).

Reverse transcriptase PCR

Total RNA was extracted from cell pellets using the TRIzol reagent (Invitrogen). The reverse transcriptase PCR (RT-PCR) was performed using a High Capacity cDNA Reverse Transcription Kit (Applied Biosystems) according to the manufacturer's instructions with primers for human D6 (forward: 5′-GGGTTTCTCCTTCCACTCCT-3′; reverse: 5′-TATTCCCCACATCCTCCTTG-3′) and human β-actin (forward: 5′-GCTCGTCGTCGACAACGGCT-3′; reverse 5′-CAAACATGATCTGGGTCATCTTCTCT-3′). TaqMan real-time RT-PCR was used to detect D6 RNA in KS-IMM seeded in DMEM 1% FCS overnight and stimulated for 8 or 24 hours with UO126 (10 μmol/L; Calbiochem) and PLX4032 (1 μmol/L; Selleckchem).

Chemokine scavenging assay

KS-IMM transfectants were plated the day before the experiment in 96-well plates (3×10^4 cells/well), and then incubated with 10 ng/mL of CCL3L1 (R&D Systems) for increasing times. The supernatant was collected and the chemokine concentration was evaluated by sandwich ELISA (R&D Systems).

Published OnlineFirst April 2, 2014; DOI: 10.1158/2326-6066.CIR-13-0202

Bone marrow–derived macrophages

Bone marrow cells were obtained from femurs of 8-week-old male wild-type (WT) and CCR2$^{-/-}$ C57/Bl6 mice and plated in DMEM with 5% FCS for 4 hours at 37°C. Nonadherent cells were recovered and plated at 3×10^5 cells per well in 24-well ultra-low attachment plates (Corning Costar) and cultured for 7 days in the presence of 25% conditioned media from D6$^-$KS or D6$^+$KS cells or with 20 ng/mL murine macrophage (mM)-colony-stimulating factor (mM-CSF; Miltenyi Biotec) added every 2 days. When indicated, indomethacin (Sigma) was added to cultures at 10 μmol/L from day 0. After 7 days, cells were detached with cold Accutase (Millipore).

In vivo experiments

WT and CCR2$^{-/-}$ C57/Bl6 mice and nude CD-1 mice were purchased from The Jackson Laboratory and Charles River Italia, respectively. Animals were housed in pathogen-free conditions, and used at 8 to 12 weeks of age. Mice were injected subcutaneously in the flank with 5×10^6 KS-IMM cells mixed with liquid Matrigel (BD Biosciences). The two major tumor diameters were measured every 2 to 3 days with a caliper, and the tumor volume was estimated by applying the formula $(d_1 \times d_2^2)/2$. To deplete neutrophils *in vivo*, purified anti-Ly6G rat mAb (clone 1A8; BioXCell) was administered to mice (intraperitoneally; 0.2 mg) 1 day before KS-IMM inoculation and every 3 days thereafter. Control animals received purified whole rat immunoglobulin G2a (IgG2a; BioXCell). Pharmacologic inhibition of CCR2 was achieved by treating mice daily with 2 mg/kg RS-504393 (Santa Cruz Biotechnology) via oral gavage from the day of KS-IMM injection until the day the animals were sacrificed. In some experiments, bone marrow–derived macrophages (BMDM; 10 ng/mL mM-CSF) generated from WT and CCR2$^{-/-}$ C57/Bl6 mice were mixed in liquid Matrigel at 1:2 ratio with KS-IMM cells and subcutaneously injected. Animal housing and procedures were in accordance with national (D.L. N.116, reviewed and approved Gazzetta Ufficiale della Repubblica Italiana, supplement 40, 18-2-1992) and international law and policies (European Economic Community Council, 1987, Directive 86/609, Official Journal of European Community L 358.1; and Institute of Laboratory Animal Resources, Committee on Life Sciences, National Research Council, 1996, Guide for the Care and Use of Laboratory Animals). Animal procedures were also reviewed and approved by the Institutional Ethical Committee at Humanitas Clinical and Research Center (Rozzano, Italy).

Fluorescence-activated cell sorting analysis and sorting

Flow cytometry was performed using FACSCanto II flow cytometer and FACSDiva 6.1.1 software (BD Biosciences) or FlowJo (TreeStar). KS-IMM cells were sorted for enhanced GFP (EGFP) expression by using a FACSAria flow cytometer (BD Biosciences). For tumor infiltrate analysis, tumor explants were harvested at the indicated time points, minced and incubated in DMEM with 1% FCS plus collagenase IV (Sigma-Aldrich Chemicals) for 30 minutes at 37°C, and then passed through a 70-μm nylon mesh filter (BD Falcon). Erythrocytes were lysed with ammonium–chloride–potassium buffer. Cells were stained with anti-mouse CD45-PercP, CD11b-APC, Ly6G-PE, Ly6C-FITC, I-A/I-E-Biotin, anti-CD206-Biotin (BD Biosciences), and F4/80 (Serotec). Dead cells were excluded by the LIVE/DEAD Fixable Cell Stain Kit (Invitrogen). The absolute number was determined using TruCount beads (BD Biosciences) according to the manufacturer's instructions.

Cytokine levels and migration assay

KS-IMM cells were seeded into 24-well microplates (9×10^5 cells/well) and grown under normal conditions for 24 hours. The medium was replaced by DMEM with 1% FCS, and in a particular experiment 10 ng/mL of human IL (hIL)-1β (R&D Systems) were added. Supernatants were collected after 24 hours and hCCL2, hIL-6, and hVEGF-A were measured using sandwich ELISA (R&D Systems). mVEGF-A was measured in tumor lysates and BMDM supernatants using ELISA test (R&D Systems) and murine chemokines using Bio-Plex protein assay (Bio-Rad). Human monocyte isolation and migration toward D6$^-$KS or D6$^+$KS tumor-conditioned medium (TCM) were performed as previously described (32).

Western blot analysis

Cells (0.7×10^6) were treated as indicated and lysed with a buffer containing 50 mmol/L Tris–HCl (pH 8), 150 mmol/L NaCl, 5 mmol/L EDTA, 1.5 mmol/L $MgCl_2$, 10% glycerol, 1% Triton X-100, and protease/phosphatase inhibitors. The lysates were electrophoresed and immunoblotted with the rabbit anti-human ph-ERK1/2 antibody (Cell Signaling Technology) using standard conditions. Chemiluminescence was acquired by the ChemiDoc XRS Imaging System, densitometric analysis was performed by Image Lab software (Bio-Rad), and the protein band intensity was calculated by normalizing against the α-tubulin band intensity.

Statistical analysis

Data were compared using an unpaired Student t test. Immunohistochemical data were analyzed by the two-tailed unpaired t test with Welch correction (GraphPad Prism4 software). *, $P < 0.05$; **, $P < 0.005$; ***, $P < 0.0005$. Linear regression analysis was obtained using Prism4 software.

Results

D6 is expressed in KS lesions

D6 was reported to be expressed by LECs (12), which are precursors of KS spindle cells (13); we investigated D6 expression in KS lesions. D6 expression was readily detectable in indolent cutaneous nodular lesions of HIV-seronegative patients and, to significantly lower levels, in aggressive lesions in HIV-seropositive patients (Fig. 1A). When biopsies of maculonodular lesions of HIV-seronegative patients were analyzed, D6 expression was significantly higher in patients who showed a slow disease progression rate (stage IA) than in those characterized by a rapid progression rate (stage IB; Fig. 1B; ref. 19). D6 staining was observed in a large fraction of spindle-shaped tumor cells, which were also positive for the HHV8-encoded nuclear antigen LANA-1 (Fig. 1C).

D6 expression restrains KS growth *in vivo*

To determine the role of D6 in KS, we used the human cell line KS-IMM, originally derived from a biopsy of an iatrogenic

Published OnlineFirst April 2, 2014; DOI: 10.1158/2326-6066.CIR-13-0202

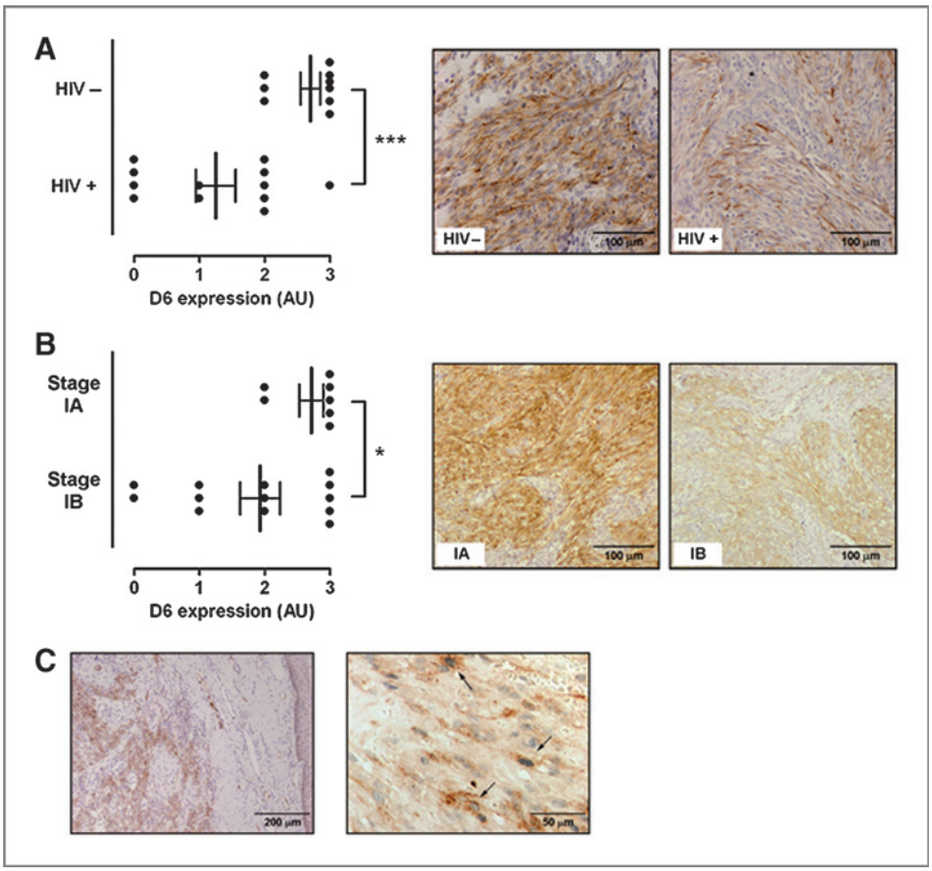

Figure 1. D6 expression in human KS lesions and KS-associated HHV8$^+$ spindle cells. D6 immunohistochemical analysis in cutaneous maculonodular KS lesions from (A) HIV-seropositive and -seronegative patients ($n = 22$) and (B) from HIV-seronegative patients affected by disease with slow (stage IA) and rapid (stage IB) progression rate ($n = 21$). Representative panels of D6 staining are shown on the right (magnification, ×20). Scatter plots report mean ± SEM from five random fields evaluated for number of positive cells using a semiquantitative scale (0, no positive cells; 1, 0%–25% positive cells; 2, 25%–75% positive cells; and 3, >75% positive cells). C, a representative immunohistochemical analysis of a cutaneous KS lesion from an HIV-seronegative patient stained for human D6 (brown) and LANA-1 (blue). KS spindle cells are indicated by arrows. Magnification, ×10 (left) and ×40 (right). *, $P < 0.05$; ***, $P < 0.0005$.

KS that was able to grow in nude mice as highly vascularized tumors closely resembling human KS lesions (31). As KS-IMM cells were negative for D6 expression (Supplementary Fig. S1A), their expression was reconstituted by transfection. D6 expression in D6$^+$KS was confirmed by RT-PCR (Supplementary Fig. S1A) and fluorescence microscopy (Supplementary Fig. S1B), which also showed predominant localization of D6 in intracellular perinuclear compartments, consistent with the distribution of D6 observed in KS spindle cells (Fig. 1C) and other D6 transfectants (33). D6 was functional, as D6$^+$KS but not D6$^-$KS cells internalized and degraded exogenously provided chemokines (Supplementary Fig. S1C). D6$^-$KS supernatant contained higher levels of hCCL2 (Supplementary Fig. S1F) and exhibited higher chemotactic activity for monocytes as compared with D6$^+$KS supernatant (Supplementary Fig. S1G), indicating that D6 expression affected the chemotactic potential of KS cells. Consistent with the D6 specificity for chemokines, no difference was found in the amount of IL-6 and VEGF-A detected in the supernatant of D6$^+$KS and D6$^-$KS cells (Supplementary Fig. S1D and S1E, respectively). Finally, no difference was found in the growth rate of D6$^-$KS and D6$^+$KS cells (Supplementary Fig. S1F). D6-transfected KS-IMM cells express a fully functional D6 scavenger receptor, which has an impact on the chemokine milieu but not on the production of other cytokines or on cell growth *in vitro*.

The role of D6 *in vivo* was investigated by implanting three independent populations of D6$^+$KS and D6$^-$KS cells in the flanks of CD-1 nude mice (Fig. 2A and B, respectively). Up to day 19 after injection, the two groups of animals showed comparable tumor uptake and similar tumor growth. However, from day 19 onward, D6$^-$KS tumors were significantly larger than D6$^+$KS tumors and, at the conclusion of the experiment, they were on average 2.77 ± 1.28 times bigger than D6$^+$KS tumors, suggesting that the lack of D6 expression allows an increased tumor growth rate *in vivo* (Fig. 2C). An analysis of the necrotic area at this time point by hematoxylin and eosin staining showed no difference between D6$^+$KS and D6$^-$KS tumors (Supplementary Fig. S2), indicating that the greater tumor size of D6$^-$KS was not due to higher necrosis, as previously reported for other atypical chemokine receptors (34).

Higher levels of inflammatory chemokines and M2-like tumor-associated macrophages infiltrate in D6$^-$KS

To dissect the mechanism by which D6 restrains KS growth *in vivo*, lysates of D6$^-$KS and D6$^+$KS tumors were analyzed for their chemokine content. When compared with D6$^+$KS lysates, D6$^-$KS lysates contained a higher amount of host-derived mCCL2, mCCL5, and mCCL3 (Fig. 3A–C, respectively). Very low concentrations of hCCL2 were detected (data not shown), indicating that the main source of chemokines in the system was infiltrating host cells rather than tumor cells, as reported for some human tumors (11).

When the explanted tumors were analyzed for their cellular composition by flow cytometry analysis, tumor masses were

Published OnlineFirst April 2, 2014; DOI: 10.1158/2326-6066.CIR-13-0202

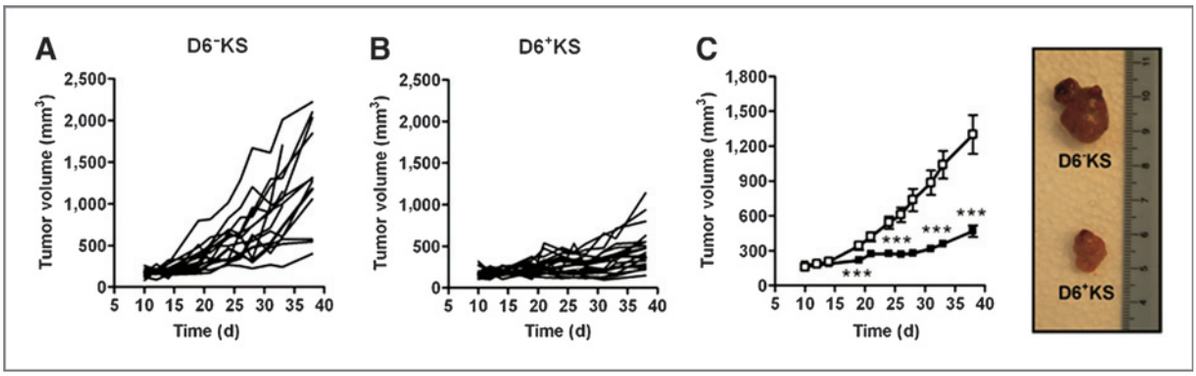

Figure 2. D6 expression restrains KS tumor growth *in vivo*. A and B, growth rate of tumors generated in the flank of each CD-1 nude mouse injected with 5×10^6 D6$^-$KS ($n = 23$) or D6$^+$KS ($n = 17$) cells, respectively. C, average volumes ± SEM of tumors derived from D6$^+$KS (■) and D6$^-$KS (□). Representative tumor explants derived from D6$^-$KS (top) and D6$^+$KS (bottom) are shown on the side. ***, $P < 0.0005$.

composed of equal amounts of tumor cells (EGFP$^+$ and CD45$^-$) and infiltrating leukocytes (EGFP$^-$/CD45$^+$). Stromal cells (EGFP$^-$/CD45$^-$) represented less than 5% of the tumor mass (Fig. 3D). Expression of D6 not only had a significant impact on the number of tumor cells and infiltrating leukocytes (Fig. 3E and F, respectively), but it also had qualitative effects on the infiltrating leukocytes. In the absence of D6, KS tumors showed a significant increase in infiltrating neutrophils (CD11b$^+$, Ly6C^{int}, F4/80$^-$, and Ly6G$^+$; Fig. 3G) and tumor-associated macrophages (TAM; R3: CD11b$^+$, Ly6C$^-$, F4/80^{++}; Fig. 3H), while they contained a reduced number of monocytes (R1, CD11b$^+$, Ly6C^{high}, and F4/80$^-$; R2, CD11b$^+$, Ly6C^{high}, and F4/80$^+$). TAMs were then analyzed for the expression of the M1 marker MHC-II and the M2 marker mannose receptor (also known as CD206). Compared with D6$^+$KS, TAMs infiltrating D6$^-$KS tumors had decreased levels of MHC-II and a tendency to have more CD206 (Fig. 3I and J, respectively). Similar results were obtained with BMDM differentiated *in vitro* with TCM from D6$^+$KS or D6$^-$KS, with a higher amount/percentage of macrophages (Fig. 4A), increased levels of the M2 marker CD206 (Fig. 4C), and reduced levels of the M1 marker MHC-II (Fig. 4B) induced by TCM from D6$^-$KS as compared with TCM from D6$^+$KS cells. These data indicate that reduced levels of D6 are associated with increased TAM recruitment and their local maturation toward M2-like polarization.

TAM recruitment is required for KS growth

To assess the role of the tumor-infiltrating leukocytes on KS growth, depletion experiments were performed. Treatment with the anti-Ly6G 1A8 mAb efficiently depleted circulating polymorphonuclear leukocytes (PMN; Fig. 5A) and abolished their infiltration in KS tumors (Fig. 5B), but had no effect on the progression of both D6-competent and -incompetent tumors (Fig. 5C). Conversely, the reduction of circulating monocytes (Fig. 5D) and infiltrating TAMs (Fig. 5E) by treatment with the CCR2 antagonist RS-504393 had no effect on D6$^+$KS growth, but it significantly inhibited D6$^-$KS growth rate at early time points (Fig. 5F). A partial inhibition of the growth of D6$^-$KS by a CCR2 antagonist is consistent with these lesions containing increased levels of other monocyte-attracting chemokines (Fig. 3B and C). Finally, *in vivo* experiments showed that while coinjection of WT or CCR2$^{-/-}$ BMDM did not modify D6$^-$KS tumor growth (Fig. 5G), the growth of D6$^+$KS tumors was supported by the coinjection of WT but not CCR2$^{-/-}$ BMDM (Fig. 5H), indicating the relevance of CCR2 expression by TAMs for their protumor activity beyond their local recruitment.

Increased production of VEGF-A and angiogenesis in D6$^-$KS

To understand the mechanism by which TAMs promote KS growth, the content of the angiogenic factor VEGF-A and the expression of the endothelial cell marker CD31 in D6$^-$KS and D6$^+$KS tumor sections were investigated. Although no difference was found for the human VEGF-A content (data not shown), D6-incompetent tumors showed higher levels of murine VEGF-A than D6-competent tumors (Fig. 6B), and immunohistochemical analysis with anti-CD31 showed that D6$^-$KS cells were more vascularized than D6$^+$KS (Fig. 6A). The conditioned medium of D6$^-$KS but not D6$^+$KS cells increased the production of mVEGF-A by BMDM (Fig. 6C). This effect was not observed when CCR2$^{-/-}$ BMDMs were used (Fig. 6C), indicating a key role for tumor-derived CCR2 agonists in the acquisition of a proangiogenic phenotype. CCR2 agonists were described to induce VEGF-A production through an autocrine pathway requiring COX2 activity (35, 36). In agreement with this observation, the COX2 inhibitor indomethacin inhibited mVEGF-A production by BMDM stimulated with D6$^-$KS TCM (Fig. 6C).

Role of the ERK pathway in the downregulation of D6 expression

The HHV8 reactivation process in KS is associated with the activation of the K-Ras–B-Raf–MEK pathway (37), and the K-Ras–activating mutations or amplifications are frequently found in KS lesions, particularly in the advanced stages (38, 39). To investigate the connection between ERK pathway activation and D6 downregulation, we analyzed the KS-IMM cell line. Although no mutations in the K-Ras gene were detected, the B-Raf V600E oncogenic mutation was present (Fig. 7A). Consistent with the ability of activated B-Raf to phosphorylate MEK, which in turn activates the ERK1/2 pathway (40), KS-IMM showed high levels of ERK1/2 phosphorylation (Fig. 7B), which was inhibited by

Published OnlineFirst April 2, 2014; DOI: 10.1158/2326-6066.CIR-13-0202

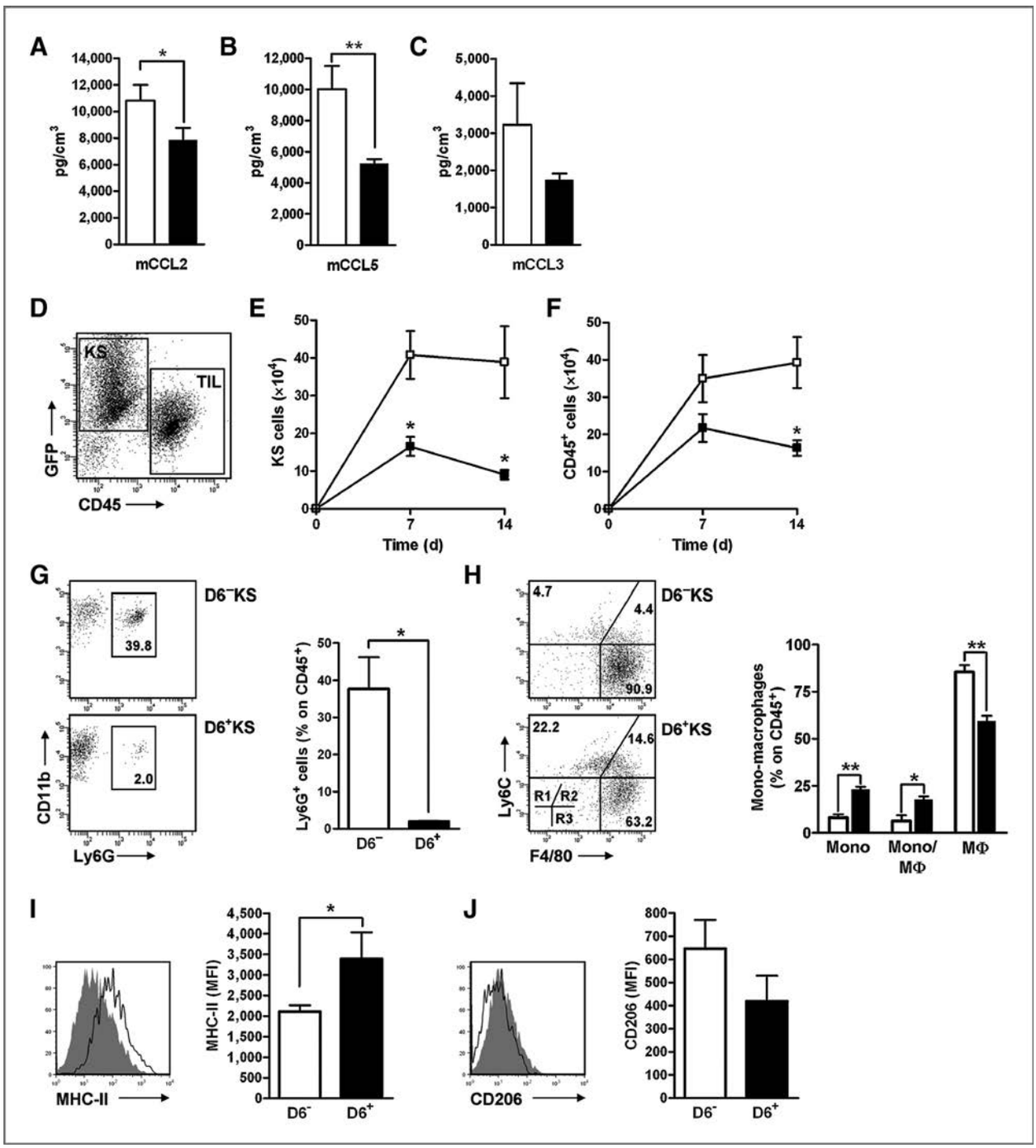

Figure 3. Increased chemokine content and leukocyte infiltrate in D6-negative tumors. (A) mCCL2, (B) mCCL5, and (C) mCCL3 were measured in homogenized tumors at day 14 after inoculation. Data are expressed as the mean concentration ± SEM of the chemokine levels normalized for the tumor volume ($n = 4$/each group). D, representative dot plot analysis of an enzymatically digested tumor stained and analyzed by flow cytometry showing gating strategy to detect tumor cells (KS) and tumor-infiltrating leukocytes (TIL) analyzing live cells and singlets in single-cell suspension for the expression of GFP and CD45. Mean ± SEM of the total number of GFP^+ KS cells (E) and $CD45^+$ infiltrating leukocytes (F) at day 7 and 14 after inoculation of $D6^+$KS (■) and $D6^-$KS (□) are shown. G, representative dot plot and mean of the percentage of $CD11b^+$ $Ly6G^+$ neutrophils in the $CD45^+$ (H) gate and monocytes (R1, $Ly6C^{high}$ and $F4/80^-$), mono-macrophages (R2, $Ly6C^{high}$ and $F4/80^+$), and macrophages (R3, $Ly6C^-$ and $F4/80^+$) in the $CD11b^+$ $Ly6G^-$ gate at day 7. Representative histogram plot and mean fluorescence intensity (MFI) of (I) MHC-II and (J) CD206 expression of R3-gated cells in $D6^+$ (black line) and $D6^-$KS (gray area) tumors. All gates are based on isotype controls. In all figures histograms represent the mean ± SEM of at least three independent experiments ($n = 5$ tumors/group) of $D6^+$KS (black bar) or $D6^-$KS (white bar). *, $P < 0.05$; **, $P < 0.005$.

Published OnlineFirst April 2, 2014; DOI: 10.1158/2326-6066.CIR-13-0202

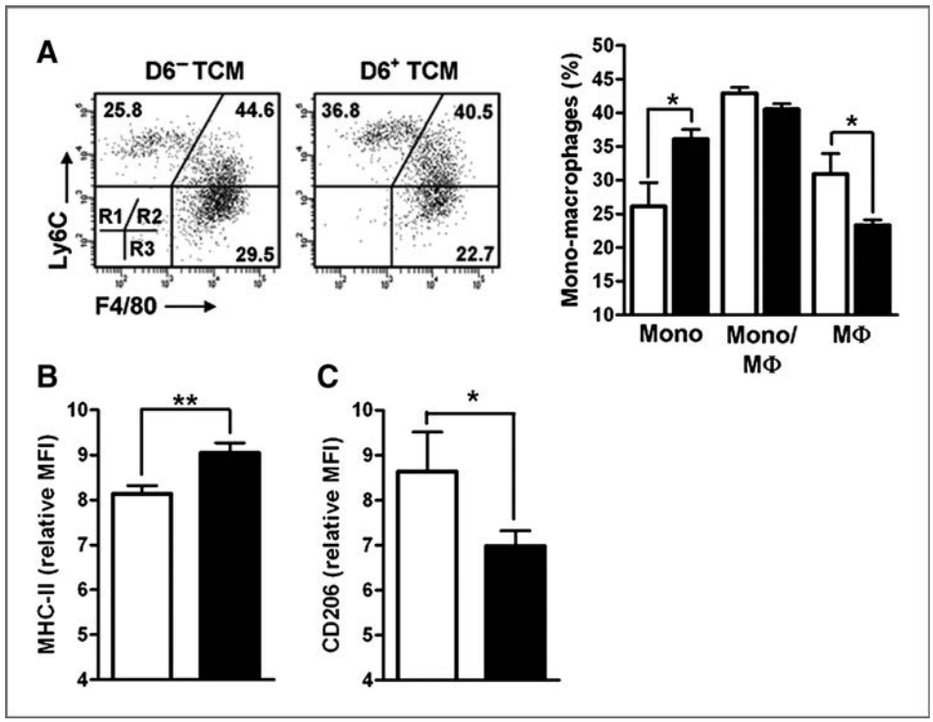

Figure 4. Increased M2-like macrophage differentiation induced by D6$^-$KS supernatant. A, representative dot plot analysis and percentage of monocytes (R1), mono-macrophages (R2), and macrophages (R3) of WT BMDM cultured with D6$^-$KS (white bar) or D6$^+$KS (black bar) TCM labeled and gated as described in Fig. 3H. Relative mean fluorescence intensity (MFI) of (B) MHC-II and (C) CD206 on R3-gated macrophages cultured with D6$^-$KS (white bar) or D6$^+$KS (black bar) TCM. Mean ± SEM of at least three independent experiments is shown. *, $P < 0.05$; **, $P < 0.005$.

the B-Raf inhibitor PLX4032 and the MEK inhibitor U0126 with a concomitant upregulation of D6 expression (Fig. 7C), indicating that D6 expression in KS-IMM is downregulated as a consequence of the constitutive activation of the B-Raf–MEK–ERK pathway.

ERK activation, macrophage infiltration, and D6 expression in human KS

To assess the actual clinical relevance of the pathway described above, ERK1/2 activation, D6 expression, and macrophage infiltration were examined in a series of patients with KS. In KS spindle cells of stage IB KS lesions, an inverse correlation was observed between ERK1/2 activation (anti-pERK staining) and D6 expression ($n = 10$; Fig. 7D; Supplementary Fig. S3). Immunohistochemical analysis showed increased infiltration of CD68$^+$ and CD163$^+$ (Fig. 7E and Supplementary Fig. S3) macrophages in KS lesions characterized by a rapid progression rate (stage IB) as compared with slow progressing ones (stage IA), and in these lesions there was also a significant inverse correlation between D6 expression levels and the number of CD68$^+$ ($P = 0.039$; $n = 18$) and CD163$^+$ cells ($P = 0.003$; $n = 18$; Fig. 7F). Taken together, these results are consistent with data obtained in the experimental model using the KS-IMM cell line and support the notion that in KS progression, activation of the B-Raf–MEK–ERK pathway mediates the downregulation of D6, resulting in increased chemokine-mediated infiltration of TAM and their local activation toward a tumor-promoting M2-like phenotype.

Discussion

Chemokines are important components of cancer-related inflammation affecting tumor progression in multiple pathways, including tumor cell proliferation and survival, invasion and metastasis, leukocyte recruitment, and angiogenesis (3, 8, 41). By targeting the degradation of most inflammatory CC chemokines and limiting their bioavailability in tissues, the atypical chemokine receptor D6 represents an emerging mechanism of regulation of the chemokine system (42). D6 has a well-established nonredundant role in the control of the inflammatory response, regulating the traffic and the activity of cells of the mononuclear system, in particular inflammatory monocytes (5), and also a negative role in inflammation-driven tumor development in experimental models (6, 7). D6 has been reported to be expressed in human choriocarcinoma cell lines (43) and in breast (44) and vascular tumors (12, 45), but its actual relevance in human cancer has not been established.

KS is a malignancy caused by the interplay of the HHV8-infected LECs, oncogenic events, and a tumor-promoting chronic inflammatory milieu (22). Considering the major role of inflammatory chemokines in KS pathogenesis and that LECs express the atypical chemokine receptor D6 (14), analysis of its expression was performed on biopsies of KS lesions. D6 was found expressed by HHV8-infected spindle-shaped KS cells, and its expression was inversely correlated with tumor aggressiveness, both when comparing maculonodular KS lesions retrospectively classified according to their progression rate (group A vs. group B stage I lesions) and when comparing maculonodular lesions of HIV-seronegative and HIV-seropositive patients, who typically show a slow and rapid progression rate, respectively.

To test the hypothesis emerging from these observations that the reduction of D6 expression might be part of the natural KS progression process, we set up an experimental model based on the tumor cell line KS-IMM, which was derived from a human

Published OnlineFirst April 2, 2014; DOI: 10.1158/2326-6066.CIR-13-0202

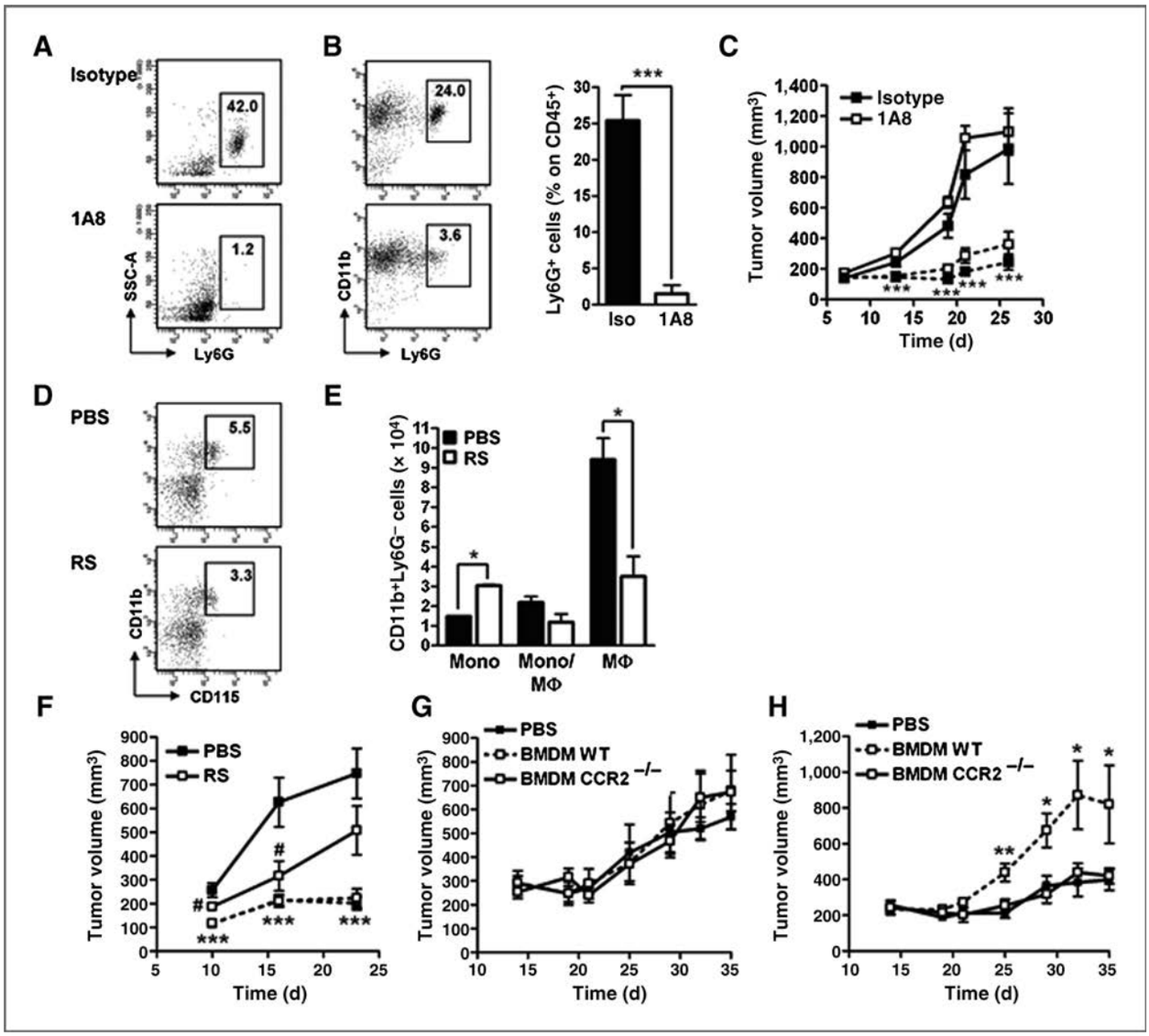

Figure 5. KS growth is sustained by TAM recruitment. Mice inoculated with D6$^-$KS or D6$^+$KS cells were treated with a blocking antibody against Ly6G (1A8) or the specific CCR2 antagonist RS-509343 (RS). Representative dot plot analysis at day 25 of (A) circulating and (B) tumor-associated PMN (CD11b$^+$ and Ly6G$^+$) from D6$^-$KS–bearing mice before and after 1A8 treatment. The graph shows the percentage ± SEM of PMN in D6$^-$KS tumors. C, D6$^-$ (solid line) and D6$^+$KS (dashed line) tumor volume after subcutaneous inoculation in PBS or 1A8-treated mice. D, representative flow cytometry gating scheme at day 25 of circulating monocytes (CD11b$^+$ and CD115$^+$). E, CD11b$^+$Ly6G$^-$ tumor infiltrate in PBS-treated versus RS-treated D6$^-$KS tumors. The monocyte-macrophage population was gated as described in Fig. 3H and number ± SEM is shown in the graph. F, D6$^-$KS (solid line) and D6$^+$KS (dashed line) tumor volumes after treatment with PBS (■) or RS (□).G and H, tumor growth of D6$^-$KS and D6$^+$KS, respectively, injected alone (■) or with WT (□, dotted line) or CCR2$^{-/-}$ BMDM (□, solid line). In all panels, data are representative of two independent experiments ($n = 8$ mice/group). Results are expressed as mean ± SEM. *, $P < 0.05$; ***, $P < 0.0005$, D6$^+$ versus D6$^-$KS; #, $P < 0.05$ treatment versus control.

KS lesion and induces KS-like sarcomas, retaining most features of the parental tumor when injected subcutaneously into nude mice (31). When compared with D6-expressing KS, D6-incompetent KS displays increased tumor growth *in vivo* but not *in vitro*, suggesting that D6 expression may influence KS growth by interfering with the tumor microenvironment. Consistent with this observation, D6-negative tumors were found to be characterized by increased levels of inflammatory chemokines and profound changes in the intratumoral leukocytic infiltrate composition. D6-negative tumors showed an increased infiltration of TAMs and tumor-associated neutrophils. Despite the fact that tumor-associated neutrophils have been reported to be important for tumor growth by activating angiogenic factors (46), the selective depletion of Ly6G$^+$ cells did not affect KS growth. Conversely, inhibition of monocyte recruitment and TAM infiltration by the use of a CCR2 antagonist inhibited the growth rate of D6$^-$KS tumors. Direct assessment of the requirement of TAMs for KS growth was demonstrated by adoptive transfer experiments showing that coinjection of BMDM promoted D6$^+$KS growth. D6 expression downregulation (in

Published OnlineFirst April 2, 2014; DOI: 10.1158/2326-6066.CIR-13-0202

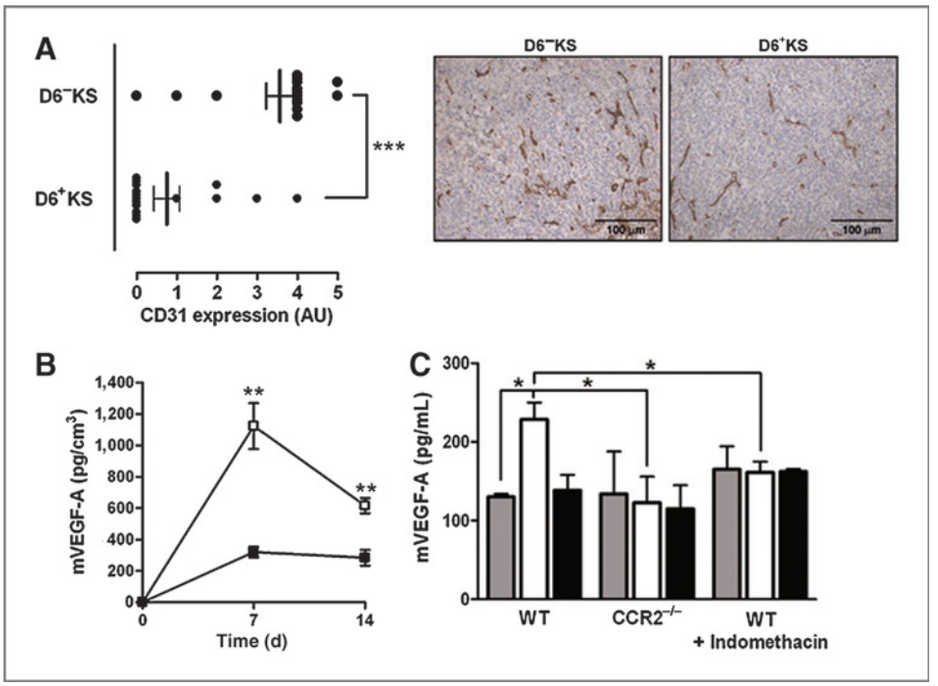

Figure 6. CCR2$^+$ TAMs sustain angiogenesis in D6$^-$KS tumors. A, mean ± SEM of the number of CD31$^+$ cells (semiquantitative score: 0, no positive cells; 1, 0%–20% positive cells; 2, 20%–40% positive cells; 3, 40%–60% positive cells; 4, 60%–80% positive cells; and 5, >80% positive cells). Score was given as the mean from five random fields for each sample. Representative images of mCD31 immunohistochemical analysis in D6$^+$KS and D6$^-$KS tumors at day 7 after implantation are shown (magnification, ×20). B, mVEGF-A concentration in homogenized D6$^+$KS (■) and D6$^-$KS (□) tumors at indicated time points. Data are expressed as the mean ± SEM ($n = 4$/each group) normalized for the tumor volume. C, mVEGF-A production by WT and CCR2$^{-/-}$ BMDM stimulated for 6 days with D6$^+$KS (■) or D6$^-$KS (□) TCM or with normal medium (■) and where indicated with indomethacin. Mean ± SEM of at least three independent experiments is shown. Results are expressed as mean ± SEM. *, $P < 0.05$, **, $P < 0.005$, ***, $P < 0.001$.

patients' KS lesions), or absence (in the KS-IMM model) was also correlated with an increased M2-like polarization of TAMs. Furthermore, the same M2-skewed phenotype was found in BMDM cultured with TCM from D6-negative tumors. Collectively, these results indicate that downregulation of this chemokine scavenger receptor at the tumor site not only allowed inflammatory CC chemokines to recruit more monocytes but also directly promoted their protumoral M2-like polarization (47).

Several studies have indicated that TAMs have a pivotal role in the regulation of tumor angiogenesis, especially at early stages of tumor progression (48). Here, we report that D6-incompetent tumors, in addition to having more TAM, had increased amounts of VEGF-A and intratumoral angiogenesis. Using KS–conditioned media, it was found that increased VEGF-A production by BMDM required CCR2 expression and an autocrine loop triggered by CCR2 agonists involving the induction of COX2 and PGE_2 production (35, 36). Furthermore, the requirement of CCR2 expression on macrophages for KS growth was directly demonstrated by adoptive transfer experiments, in which WT but not CCR2$^{-/-}$ BMDMs were able to sustain KS tumor growth. Several studies have correlated CCR2$^+$ TAM infiltration with increased tumor angiogenesis and VEGF-A production (49), but the direct role of this chemokine receptor in the production of VEGF-A has not been assessed. In addition to its known chemotactic function, we have provided evidence that CCL2 can also directly affect the angiogenic potential of TAMs; these results may be relevant to tumors other than KS that are characterized by elevated CCL2 levels, including breast and prostate tumors (11).

Oncogenic mutations or amplifications interfering with the K-Ras–B-Raf–MEK–ERK1/2 pathway are frequently observed in late-nodular KS lesions and angiosarcomas (38, 50), where its activity has been shown to support enhanced expression of growth factors and cytokines, including VEGF-A (51). Therefore, we focused on this pathway to elucidate the molecular basis responsible for D6 downregulation associated with tumor progression. Consistently with their aggressiveness *in vivo*, the KS-IMM cell line, originally established from an advanced KS lesion, harbors an activating oncogenic mutation in the B-Raf gene and shows high levels of constitutive ERK1/2 activity. In this cell system, D6 expression was found to be under the control of this signaling pathway, as its inhibition by either B-Raf or ERK inhibitors resulted in the upregulation of D6. This functional link was then confirmed in KS lesions, where D6 expression levels were found to be inversely correlated with tumor aggressiveness, ERK1/2 activation, and the number of infiltrating TAMs, for which the number and M2-like phenotype were directly correlated with tumor aggressiveness.

The results presented here suggest that during KS progression, oncogenic events activate the ERK1/2 pathway, which induces D6 downregulation in tumor cells. This allows tumor-derived inflammatory chemokines, and in particular CCR2 ligands, to recruit monocytes and sustain their local polarization toward M2-like TAMs, which support a VEGF-A–dependent angiogenic

Published OnlineFirst April 2, 2014; DOI: 10.1158/2326-6066.CIR-13-0202

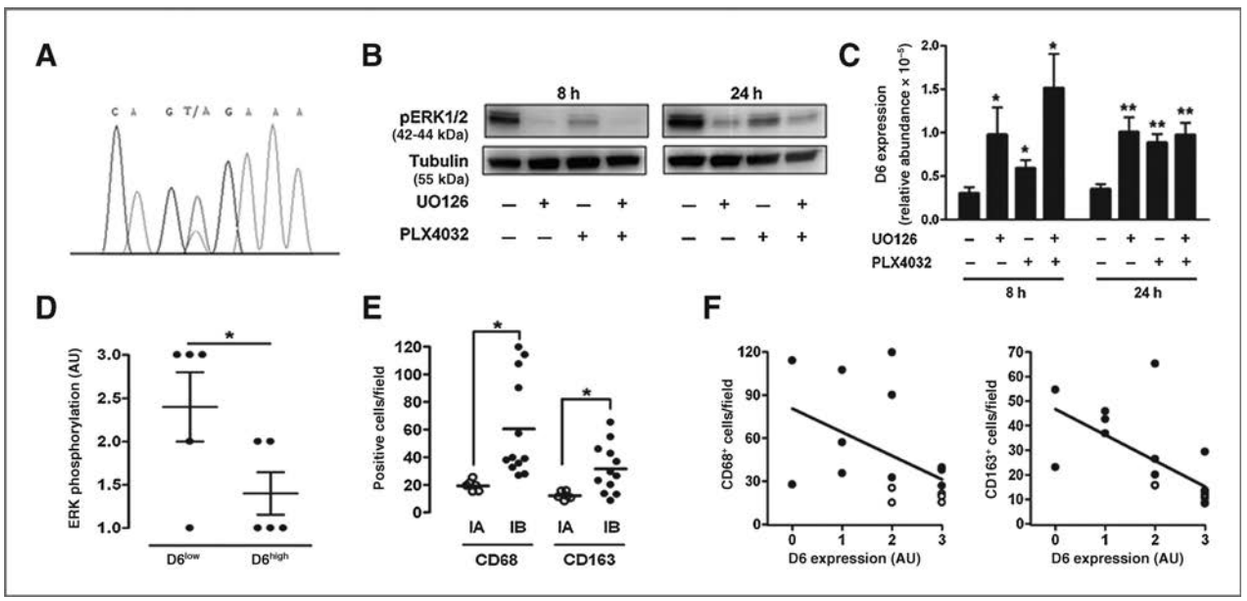

Figure 7. Downregulation of D6 expression by ERK activation. A, sequence chromatogram of BRAF exon 15 of DNA from KS-IMM cells. The thymine- (T)- to-adenine (A) transition introduces a substitution of amino acid valine to glutamic acid at codon 600 (V600E). B, Western blot analysis of ERK1/2 phosphorylation and C, qRT-PCR of D6 expression in KS-IMM cells treated with UO126, PLX4023, or their combination. D, D6 and pERK1/2 immunohistochemical analysis in cutaneous maculonodular KS lesions from stage IB patients. Scatter plot indicates mean ± SEM from five random fields evaluated for number of pERK1/2-positive cells using a semiquantitative scale (1, 0%–25% positive cells; 2, 25%–50% positive cells; 3, 50%–75% positive cells; and 4, 75%–100% positive cells) in $D6^{low}$ (score 1–2) and $D6^{high}$ (score 3–4) lesions. E, mean and SEM of CD68- and CD163-positive cells in maculonodular lesions from HIV-negative patients with slow (stage IA) and rapid (stage IB) progression rate. Five random fields for each sample were counted. F, linear regression analysis of D6 expression levels and CD68 (left) and CD163 (right) number of positive cells/fields in cutaneous maculonodular KS lesions from stage IA (○) and IB patients (●). *, $P < 0.05$; **, $P < 0.005$.

switch promoting tumor growth. Targeting these components of the KS tumor microenvironment may represent alternative or complementary therapeutic strategies.

Disclosure of Potential Conflicts of Interest

No potential conflicts of interest were disclosed.

Authors' Contributions

Conception and design: B. Savino, N. Caronni, R. Bonecchi
Development of methodology: B. Savino, N. Caronni, L. Laghi, A. Tourlaki
Acquisition of data (provided animals, acquired and managed patients, provided facilities, etc.): B. Savino, N. Caronni, A. Anselmo, F. Pasqualini, E.M. Borroni, G. Basso, G. Celesti, A. Tourlaki, V. Boneschi, L. Brambilla, M. Nebuloni, G. Vago
Analysis and interpretation of data (e.g., statistical analysis, biostatistics, computational analysis): B. Savino, N. Caronni, A. Anselmo, F. Pasqualini, L. Brambilla, G. Vago, R. Bonecchi
Writing, review, and/or revision of the manuscript: B. Savino, N. Caronni, F. Pasqualini, M. Locati, R. Bonecchi
Administrative, technical, or material support (i.e., reporting or organizing data, constructing databases): N. Caronni, F. Pasqualini, A. Tourlaki
Study supervision: G. Vago, A. Mantovani, M. Locati, R. Bonecchi

Acknowledgments

The authors thank Dr. Adriana Albini (IRCCS MultiMedica, Science and Technology Pole, Milan, Italy) for providing the KS-IMM cell line.

Grant Support

Research activities in the laboratory are supported by Ministero dell'Istruzione dell'Università e della Ricerca (PRIN and FIRB projects), Ministero della Salute (Ricerca Finalizzata), the Italian Association for Cancer Research (AIRC), and the European Community's Seventh Framework Programme [FP7-2007-2013] under grant agreement HEALTH-F4-2011-281608 (TIMER).

The costs of publication of this article were defrayed in part by the payment of page charges. This article must therefore be hereby marked *advertisement* in accordance with 18 U.S.C. Section 1734 solely to indicate this fact.

Received November 13, 2013; revised February 17, 2014; accepted March 2, 2014; published OnlineFirst April 2, 2014.

References

1. Bonecchi R, Galliera E, Borroni EM, Corsi MM, Locati M, Mantovani A. Chemokines and chemokine receptors: an overview. Front Biosci 2009;14:540–51.
2. Mantovani A. The chemokine system: redundancy for robust outputs. Immunol Today 1999;20:254–7.
3. Bonecchi R, Savino B, Borroni EM, Mantovani A, Locati M. Chemokine decoy receptors: structure-function and biological properties. Curr Top Microbiol Immunol 2010;341:15–36.
4. Mantovani A, Bonecchi R, Locati M. Tuning inflammation and immunity by chemokine sequestration: decoys and more. Nat Rev Immunol 2006;6:907–18.
5. Savino B, Castor MG, Caronni N, Sarukhan A, Anselmo A, Buracchi C, et al. Control of murine Ly6C(high) monocyte traffic and immunosuppressive activities by atypical chemokine receptor D6. Blood 2012; 119:5250–60.
6. Nibbs RJ, Gilchrist DS, King V, Ferra A, Forrow S, Hunter KD, et al. The atypical chemokine receptor D6 suppresses the development of chemically induced skin tumors. J Clin Invest 2007;117:1884–92.
7. Vetrano S, Borroni EM, Sarukhan A, Savino B, Bonecchi R, Correale C, et al. The lymphatic system controls intestinal inflammation and inflammation-associated colon cancer through the chemokine decoy receptor D6. Gut 2010;59:197–206.

Published OnlineFirst April 2, 2014; DOI: 10.1158/2326-6066.CIR-13-0202

8. Balkwill F. Cancer and the chemokine network. Nat Rev Cancer 2004;4:540–50.
9. Lazennec G, Richmond A. Chemokines and chemokine receptors: new insights into cancer-related inflammation. Trends Mol Med 2010;16:133–44.
10. Mantovani A, Allavena P, Sica A, Balkwill F. Cancer-related inflammation. Nature 2008;454:436–44.
11. Mantovani A, Savino B, Locati M, Zammataro L, Allavena P, Bonecchi R. The chemokine system in cancer biology and therapy. Cytokine Growth Factor Rev 2010;21:27–39.
12. Nibbs RJ, Kriehuber E, Ponath PD, Parent D, Qin S, Campbell JD, et al. The beta-chemokine receptor D6 is expressed by lymphatic endothelium and a subset of vascular tumors. Am J Pathol 2001;158:867–77.
13. Pyakurel P, Pak F, Mwakigonja AR, Kaaya E, Heiden T, Biberfeld P. Lymphatic and vascular origin of Kaposi's sarcoma spindle cells during tumor development. Int J Cancer 2006;119:1262–7.
14. Aguilar B, Choi I, Choi D, Chung HK, Lee S, Yoo J, et al. Lymphatic reprogramming by Kaposi sarcoma herpes virus promotes the oncogenic activity of the virus-encoded G-protein–coupled receptor. Cancer Res 2012;72:5833–42.
15. Uldrick TS, Whitby D. Update on KSHV epidemiology, Kaposi Sarcoma pathogenesis, and treatment of Kaposi Sarcoma. Cancer Lett 2011;305:150–62.
16. Mesri EA, Cesarman E, Boshoff C. Kaposi's sarcoma and its associated herpesvirus. Nat Rev Cancer 2010;10:707–19.
17. Casper C. The increasing burden of HIV-associated malignancies in resource-limited regions. Annu Rev Med 2011;62:157–70.
18. Ganem D. KSHV and the pathogenesis of Kaposi sarcoma: listening to human biology and medicine. J Clin Invest 2010;120:939–49.
19. Brambilla L, Boneschi V, Taglioni M, Ferrucci S. Staging of classic Kaposi's sarcoma: a useful tool for therapeutic choices. Eur J Dermatol 2003;13:83–6.
20. Pantanowitz L, Moses AV, Dezube BJ. The inflammatory component of Kaposi sarcoma. Exp Mol Pathol 2009;87:163–5.
21. Cesarman E, Mesri EA, Gershengorn MC. Viral G protein–coupled receptor and Kaposi's sarcoma: a model of paracrine neoplasia? J Exp Med 2000;191:417–22.
22. Ensoli B, Sturzl M. Kaposi's sarcoma: a result of the interplay among inflammatory cytokines, angiogenic factors and viral agents. Cytokine Growth Factor Rev 1998;9:63–83.
23. Douglas JL, Gustin JK, Moses AV, Dezube BJ, Pantanowitz L. Kaposi sarcoma pathogenesis: a triad of viral infection, oncogenesis and chronic inflammation. Transl Biomed 2010;1:pii:172.
24. Jensen KK, Lira SA. Chemokines and Kaposi's sarcoma. Semin Cancer Biol 2004;14:187–94.
25. Yang TY, Chen SC, Leach MW, Manfra D, Homey B, Wiekowski M, et al. Transgenic expression of the chemokine receptor encoded by human herpesvirus 8 induces an angioproliferative disease resembling Kaposi's sarcoma. J Exp Med 2000;191:445–54.
26. Bonecchi R, Bianchi G, Bordignon PP, D'Ambrosio D, Lang R, Borsatti A, et al. Differential expression of chemokine receptors and chemotactic responsiveness of type 1 T helper cells (Th1s) and Th2s. J Exp Med 1998;187:129–34.
27. D'Ambrosio D, Iellem A, Bonecchi R, Mazzeo D, Sozzani S, Mantovani A, et al. Selective up-regulation of chemokine receptors CCR4 and CCR8 upon activation of polarized human type 2 Th cells. J Immunol 1998;161:5111–5.
28. Caselli E, Fiorentini S, Amici C, Di Luca D, Caruso A, Santoro MG. Human herpesvirus 8 acute infection of endothelial cells induces monocyte chemoattractant protein 1–dependent capillary-like structure formation: role of the IKK/NF-kappaB pathway. Blood 2007;109:2718–26.
29. Xu Y, Ganem D. Induction of chemokine production by latent Kaposi's sarcoma-associated herpesvirus infection of endothelial cells. J Gen Virol 2007;88:46–50.
30. Vecchi A, Garlanda C, Lampugnani MG, Resnati M, Matteucci C, Stoppacciaro A, et al. Monoclonal antibodies specific for endothelial cells of mouse blood vessels. Their application in the identification of adult and embryonic endothelium. Eur J Cell Biol 1994;63:247–54.
31. Albini A, Paglieri I, Orengo G, Carlone S, Aluigi MG, DeMarchi R, et al. The beta-core fragment of human chorionic gonadotrophin inhibits growth of Kaposi's sarcoma-derived cells and a new immortalized Kaposi's sarcoma cell line. AIDS 1997;11:713–21.
32. Bonecchi R, Facchetti F, Dusi S, Luini W, Lissandrini D, Simmelink M, et al. Induction of functional IL-8 receptors by IL-4 and IL-13 in human monocytes. J Immunol 2000;164:3862–9.
33. Bonecchi R, Borroni EM, Anselmo A, Doni A, Savino B, Mirolo M, et al. Regulation of D6 chemokine scavenging activity by ligand- and Rab11-dependent surface up-regulation. Blood 2008;112:493–503.
34. Addison CL, Belperio JA, Burdick MD, Strieter RM. Overexpression of the duffy antigen receptor for chemokines (DARC) by NSCLC tumor cells results in increased tumor necrosis. BMC Cancer 2004;4:28.
35. Popivanova BK, Kostadinova FI, Furuichi K, Shamekh MM, Kondo T, Wada T, et al. Blockade of a chemokine, CCL2, reduces chronic colitis-associated carcinogenesis in mice. Cancer Res 2009;69:7884–92.
36. Futagami S, Tatsuguchi A, Hiratsuka T, Shindo T, Horie A, Hamamoto T, et al. Monocyte chemoattractant protein 1 and CD40 ligation have a synergistic effect on vascular endothelial growth factor production through cyclooxygenase 2 upregulation in gastric cancer. J Gastroenterol 2008;43:216–24.
37. Yu F, Harada JN, Brown HJ, Deng H, Song MJ, Wu TT, et al. Systematic identification of cellular signals reactivating Kaposi sarcoma–associated herpesvirus. PLoS Pathog 2007;3:e44.
38. Nicolaides A, Huang YQ, Li JJ, Zhang WG, Friedman-Kien AE. Gene amplification and multiple mutations of the K-ras oncogene in Kaposi's sarcoma. Anticancer Res 1994;14:921–6.
39. Spandidos DA, Kaloterakis A, Yiagnisis M, Varatsos A, Field JK. Ras, C-myc and C-erbB-2 oncoprotein expression in non-AIDS Mediterranean Kaposi's sarcoma. Anticancer Res 1990;10:1619–25.
40. Lee S, Kang J, Cho M, Seo E, Choi H, Kim E, et al. Profiling of transcripts and proteins modulated by K-ras oncogene in the lung tissues of K-ras transgenic mice by omics approaches. Int J Oncol 2009;34:161–72.
41. Bonecchi R, Locati M, Mantovani A. Chemokines and cancer: a fatal attraction. Cancer Cell 2011;19:434–5.
42. Cancellieri C, Caronni N, Vacchini A, Savino B, Borroni EM, Locati M, et al. Review: structure-function and biological properties of the atypical chemokine receptor D6. Mol Immunol 2013;55:87–93.
43. Martinez de la Torre Y, Buracchi C, Borroni EM, Dupor J, Bonecchi R, Nebuloni M, et al. Protection against inflammation- and autoantibody-caused fetal loss by the chemokine decoy receptor D6. Proc Natl Acad Sci U S A 2007;104:2319–24.
44. Wu FY, Ou ZL, Feng LY, Luo JM, Wang LP, Shen ZZ, et al. Chemokine decoy receptor d6 plays a negative role in human breast cancer. Mol Cancer Res 2008;6:1276–88.
45. McKimmie CS, Singh MD, Hewit K, Lopez-Franco O, Le Brocq M, Rose-John S, et al. An analysis of the function and expression of D6 on lymphatic endothelial cells. Blood 2013;121:3768–77.
46. Tazzyman S, Lewis CE, Murdoch C. Neutrophils: key mediators of tumour angiogenesis. Int J Exp Pathol 2009;90:222–31.
47. Roca H, Varsos ZS, Sud S, Craig MJ, Ying C, Pienta KJ. CCL2 and interleukin-6 promote survival of human CD11b^{+} peripheral blood mononuclear cells and induce M2-type macrophage polarization. J Biol Chem 2009;284:34342–54.
48. Murdoch C, Muthana M, Coffelt SB, Lewis CE. The role of myeloid cells in the promotion of tumour angiogenesis. Nat Rev Cancer 2008;8:618–31.
49. Qian BZ, Li J, Zhang H, Kitamura T, Zhang J, Campion LR, et al. CCL2 recruits inflammatory monocytes to facilitate breast-tumour metastasis. Nature 2012;475:222–5.
50. Bajaj A, Zheng Q, Adam A, Vincent P, Pumiglia K. Activation of endothelial ras signaling bypasses senescence and causes abnormal vascular morphogenesis. Cancer Res 2010;70:3803–12.
51. Akula SM, Ford PW, Whitman AG, Hamden KE, Bryan BA, Cook PP, et al. B-Raf–dependent expression of vascular endothelial growth factor-A in Kaposi sarcoma-associated herpesvirus-infected human B cells. Blood 2005;105:4516–22.

Published OnlineFirst April 2, 2014; DOI: 10.1158/2326-6066.CIR-13-0202

Cancer Immunology Research

ERK-Dependent Downregulation of the Atypical Chemokine Receptor D6 Drives Tumor Aggressiveness in Kaposi Sarcoma

Benedetta Savino, Nicoletta Caronni, Achille Anselmo, et al.

Cancer Immunol Res 2014;2:679-689. Published OnlineFirst April 2, 2014.